Characterization of Arabinoxylan −Dehydrogenation Polymer (Synthetic Lignin Polymer) Nanoparticles

5 AUTHORS, INCLUDING:

Abdellatif Barakat

French National Institute for Agricultural Res…

54 PUBLICATIONS **665** CITATIONS

SEE PROFILE

Jean-Luc Putaux

French National Centre for Scientific Research

178 PUBLICATIONS **5,167** CITATIONS

SEE PROFILE

Luc Saulnier

French National Institute for Agricultural Res…

146 PUBLICATIONS **3,991** CITATIONS

SEE PROFILE

Brigitte Chabbert

French National Institute for Agricultural Res…

99 PUBLICATIONS **3,068** CITATIONS

SEE PROFILE

Characterization of Arabinoxylan−Dehydrogenation Polymer (Synthetic Lignin Polymer) Nanoparticles

Abdellatif Barakat,[†] Jean-Luc Putaux,[‡] Luc Saulnier,[§] Brigitte Chabbert,[†] and Bernard Cathala*,[§]

UMR Fractionnement des Agroressources et Emballages, Centre de Recherche en Environnement et Agronomie, Institut National de la Recherche Agronomique, 2 Esplanade R. Garros, 51686 Reims Cedex, France, Centre de Recherches sur les Macromolécules Végétales, affiliated with Université Joseph Fourier and member of the Institut de Chimie Moléculaire de Grenoble, BP 53, F-38041 Grenoble Cedex 9, France, and Unité Biopolymères, Interactions et Assemblages, Institut National de la Recherche Agronomique, Rue de la Géraudière, BP 71627, F-44316 Nantes Cedex, France

Coniferyl alcohol (G monomer) and a mixture of coniferyl alcohol/sinapyl alcohol (GS monomers, 1/1 ratio) were polymerized to dehydrogenation polymers (DHPs) in presence of two structurally related heteroxylans (HX) differing only in their phenolic substitution patterns. One (HX-40) was enriched in ferulate (FA) while the other (HX-90) was almost devoid of FA. The morphology of the resulting nanoparticles was studied by transmission electron microscopy whereas formation of particles was followed by size exclusion chromatography with online multiangle laser light scattering. HX-40−DHP-G- and HX-40−DHP-GS-derived particles display complex morphological patterns whereas HX-90−DHP-G and HX-90−DHP-GS present rather spherical shapes. The determination of particle sizes and molar masses showed that HX-90 samples formed denser particles than HX-40 ones. These differences are discussed in relation to the ferulate substitution level.

Introduction

Plants have developed a wide range of highly organized and hierarchical composite materials (cell walls, protein bodies, cutin, microtubules, starch granules, etc.) to achieve the multiple functions required for their development. These supramolecular assemblies provide diverse chemical structures selected throughout the evolutionary process together within an inexhaustible source of models of organization that can be an inspiration to design new materials. For instance, in secondary plant cell walls, hydrophilic polysaccharides are embedded with hydrophobic phenolic polymers during lignification to form effective composites exhibiting remarkable properties and organization.[1,2] To control these properties, it is necessary to understand the organization of the lignin−polysaccharide matrix that is closely related to the chemical composition of the elementary polymers constituting the intricate networks. Thus, it will be useful to understand the relation between chemical composition and supramolecular organization either to optimize the use of plant-based products or build bio-inspired composite materials based on biopolymers extracted from renewable resources.

Heteroxylans (HXs) are a major class of polysaccharides in cell walls. In the case of graminaceous species, HXs consist of a backbone of β-(1-4)-linked D-xylose residues substituted on O-2 or/and O-3 by short side chains mainly composed of a single arabinose residue.[3] Some of the arabinose residues are ester-linked on O-5 to ferulic acid (FA) that can react under oxidative conditions with either other FA molecules or lignin.[4,5] In the first case, covalent linkages (dehydrodimer, trimer, or tetramer)[6−8] are formed between HX chains,[9,10,11] inducing interchain connections whereas in the second case, covalent linkages between lignins and polysaccharide networks are created via ferulate.[5,12] Both events are thought to have a significant impact on the lignification process and the final properties of cell walls. Indeed, lignification, the final step of the secondary cell wall formation, is an enzymatically initiated but chemically driven reaction and thus intimately depends on the structure of the preexisting polymerization medium (i.e., polysaccharide gel).[13,14] Previous studies have already pointed out the chemical importance of FA and more generally of phenolic acids in the organization of unlignified cell walls and their influence on lignin polymerization.[5,15−18] The chemical implication of FA in cell wall construction is now established. However the relation between the fine chemical structure and the supramolecular architecture of cell walls is not yet fully understood.

Our objective was to study how the FA substitution of HX influences the formation and the morphology of HX−DHP complexes (analogues of cell wall components). We polymerized coniferyl alcohol and a mixture of coniferyl alcohol and sinapyl alcohol in the presence of two structurally similar HXs that differed only in their phenolic substitution patterns. The morphology of the resulting nanoparticles was characterized by transmission electron microscopy (TEM) whereas the formation of particles was followed by size exclusion chromatography with online multiangle laser light scattering (SEC-MALLS) analysis. The combination of these approaches provided complementary information on both the final ultrastructure of the complexes and the evolution of the size, mass distribution of polymers, and internal density during the synthesis and in the final particles. Both approaches highlighted the importance of the

* Corresponding author. Phone: +33 240675068. Fax: +33 240675025. E-mail: cathala@nantes.inra.fr.

† Centre de Recherche en Environnement et Agronomie, Institute National de la Recherche Agronomique.

‡ Centre de Recherches sur les Macromolécules Végétales.

§ Unité Biopolymères, Interactions et Assemblages, Institut National de la Recherche Agronomique.

ferulate moiety on the building up of the supramolecular organization of the particles.

Materials and Methods

HX Extraction and Characterization. HX fractions were isolated from maize bran under mild or severe alkaline conditions using 1.5 M KOH at 40 °C for 2.5 h (HX-40) or 1% Ca(OH)$_2$ at 90 °C for 2.5 h (HX-90).[19] The maize bran was suspended in an alkaline solution (10 g/100 mL). The residue was separated by centrifugation and was rinsed with water (3 times). The extract was acidified to pH 3.5, concentrated, and dialyzed against distilled water. The pH was adjusted to 3.5, and HX samples were isolated by EtOH precipitation (3 vol, overnight at 4 °C). Recovery yields of 8.1% and 40% (wt %) were observed for extraction with KOH and Ca(OH)$_2$, respectively. HX fractions were further purified by ion exchange chromatography on a DEAE Sepharose CL-6B column as previously described.[20] HXs were loaded onto the column, and the gel was washed with 2.5 column volumes of 0.05 M NaOAc buffer, pH 4.5. The bound material was eluted with 2.5 column volumes of 0.05 M NaOAc buffer, pH 4.5. The bound fractions eluted with 0.05 M buffer were pooled, concentrated, extensively dialyzed against distilled water, and freeze-dried to give purified HX fractions (HX-40 and HX-90). Chromatographic yields were approximately 90% for both fractions.

The identification and quantification of neutral and acidic carbohydrates was carried out using high-performance anion exchange chromatography. The various samples were hydrolyzed using 1 M H$_2$SO$_4$ acids for 2 h at 100 °C. All samples were then filtered (PTFE, 0.45 μm) before injection onto a CarboPac PA-1 anion exchange column (4 × 250 mm, Dionex). Monosaccharide composition was analyzed and quantified using both L-fucose as the internal standard and standard solutions of neutral carbohydrates (L-arabinose, D-glucose, D-xylose, and D-galactose) and uronic acids (D-galacturonic and D-glucuronic acids).

Ferulic, diferulic, and *p*-coumaric acids were released by incubating 30−40 mg samples with NaOH (10 mL, 2 M) for 2 h at 35 °C with constant stirring under nitrogen. After 2 h, the reaction was stopped by adjusting the pH to 1 with 6 M HCl prior to addition of 3,4,5-trimethoxy-*trans*-cinnamic acid as an internal standard. Phenolic acids were extracted with ether (30 mL, 3 times). Ether fractions were pooled and evaporated to dryness under reduced pressure. The dried extract was dissolved in 1.5 mL of methanol−water (1:1, v/v) and filtered (0.45 μm) prior to injection on a Spherisorb S5 ODS2 (Waters, RP-18, 250 mm × 2.6 mm) column. Phenolic acids were detected using a Waters photodiode array UV detector and quantified at 302 nm.

Coniferyl and Syringyl Alcohol Synthesis. Coniferyl alcohol (4-hydroxy-3-methoxy-4-hydroxy-3,5-methoxy cinnamyl alcohols (G and S) was obtained according to the procedure described by Ludley and Ralph.[21] Coniferaldehyde and sinapaldehyde (4 g) was dissolved in ethyl acetate (250 mL) and then reduced by sodium borohydride (1.67 g, 44 mmol, 2 equiv). After overnight stirring, the yellow precipitate was poured into water (250 mL). This mixture was stirred for 1 h and then extracted by ethyl acetate (3 times). Combined organic fractions were dried over magnesium sulfate. Solvent was removed, and the solid residue was recrystallized in a dichloromethane/hexane mixture, giving a 75% yield pure coniferyl alcohol. ^{1}H NMR (CDCl$_3$, 250 MHz): 6.89 (m, 3H), 6.53 (d, 1H), 6.21 (d, 1H), 4.18 (d, 2H), 3.85 (s, 3H).

Synthesis of HX−DHP Complexes. Three solutions were prepared for the polymerization experiments. Solution A consisted of 100 mg of HX dissolved in 100 mL of phosphate buffer (30 mM, pH 5.0); solution B consisted of 100 mg of coniferyl alcohol and coniferyl/sinapyl alcohols 1/1 mixture (w/w) in 3 mL of dioxane and 22 mL of HX (1 g/L) in phosphate buffer (30 mM, pH 5.0); solution C consisted of 0.1 mL (2 equiv compared to coniferyl alcohol) of hydrogen peroxide H$_2$O$_2$ (35 wt % in water) in 25 mL of HX (1 g/L) in phosphate buffer (30 mM, pH 5.0). Polymerization was run according the Zutropfverfahren method (ZT). Solutions B and C were gradually added during

240 min to 50 mL of solution A, containing 5 mg of peroxidase (EC 1 11.1.7 purchased from Sigma 250−330 unit/mg) for 4 h at 25 °C. For the TEM observations, only the final samples were used whereas the SEC studies were done on samples taken out of the solution at 10, 30, and 60 min and at the end of the reaction.

Transmission Electron Microscopy. Drops of particle suspensions were deposited onto glow-discharged carbon-coated microscopy grids. Prior to complete drying, they were negatively stained with 2% uranyl acetate. In addition, specimens for cryo-TEM were prepared by quench-freezing thin films of the suspensions in liquid ethane.[22] They were mounted in a Gatan 626 cryo-holder and maintained at low temperature in the microscope (−180 °C). All samples were observed using a Philips CM200 "cryo" microscope operating at 80 kV. Images were recorded on Kodak SO163 films. The negatives were digitized off-line with a Kodak Megaplus CCD camera, and the particle diameter was measured using the ImageJ software.

Multidetected Size Exclusion Chromatography. Size exclusion chromatography is the most common technique to obtain information about the molar mass of polymers. It is especially adapted in the case of polydisperse samples, and the use of an online molar mass-sensitive detection method such as multiangle laser light scattering allows absolute molar mass and size determination for each slice across the sample peak. Thus it offers the possibility to fully describe the molecular distribution of the samples.

Measurements were performed on a multidetection system consisting of a UV detector (Waters 486), a refractive index detector (Waters 410), and a multiangle laser light scattering detector (Dawn MALLS, 632.8 nm, Wyatt Corporation). The MALLS detector worked simultaneously at 18 angles. Therefore, the apparatus was equipped with nine interference filters (on odd-numbered detectors) with a bandwidth of 1 nm to avoid any overestimation of measurement induced by DHP's fluorescence. The ASTRA software (Wyatt) was used for light scattering data collection during SEC runs. Typically, 100−200 μL sample solutions were injected at a concentration of 0.05−2%. Samples were filtered on a 0.45 μm PTFE filter, and percentage recoveries are reported in Table 3. Separation was performed on thermostatically controlled Shodex OH pack 802, 803, and 805 columns (each 4.6 mm × 300 mm) at 60 °C with a flow rate of 1 mL/min using NaNO$_3$ solution (50 mM) containing 0.02% of NaN$_3$. We do not detect any significant changes in the molar masses and size distributions according to the flow rate variation, volume of injection, and injected concentrations (data not shown), suggesting that no aggregation occurs or at least that, if they exist, aggregates form stable structures within the range of the physicochemical conditions used in this study.

The responses of the MALLS detectors were normalized to the 90° detector signal. The normalization of the apparatus detector was performed with two low molecular weight monodisperse pullulan standards (20 000 and 11 000 g/mol). The molar mass of the particles and the root-mean-square radius were obtained using the Berry plot procedure with a first-order fit furnished by the Astra software. Those are independent of any calibration or reference standards, but the sample concentration for each slice of the peak needs to be known. It is usually recalculated from refractive index elution profiles using the refractive index increment (dn/dC) that is a specific value related to the polymer structure and solvent. The dn/dC value of the DHP/HX mixtures changed for each reaction time since DHP and HX have different individual dn/dC and DHP/HX ratios increasing during the reaction course. However, dn/dC for each DHP/HX ratio (equivalent to reaction time) can be calculated by using a mixing law. The dn/dC values of the HX/DHP mixtures were estimated from the following calculation $(dn/dC)_{HX-DHP} = x_{HX}(dn/dC)_{HX} + x_{DHP}(dn/dC)_{DHP}$, where x_i is the weight fraction of compound i and $(dn/dC)_i$ is its refractive index increment in water. For all calculations only the odd-numbered detectors equipped with fluorescence filters were used. For HX, a dn/dC value equal to 0.146 was used in agreement with previous studies.[23] For DHPs, since they are insoluble in water, the refractive index increment was calculated from $(dn/dC)_{DHP} = [(\rho_{DHP} - \rho_{DMF})(dn/dC)_{DHP/DMF} - (\Delta n_{DMF-water})]/$

Table 1. Physicochemical Characteristics of HX Extracted from Maize Bran by Alkaline Extraction[a]

	HX-40	HX-90
carbohydrates content (%)		
neutral sugar	93.4	92.5
Ara	33.7	33.4
Xyl	51.3	51.1
Gal	8.4	8.2
uronic acids	6.6	7.5
Ara/Xyl	0.66	0.65
phenolics acid content (μg/mg)	4.85	0.29
$\overline{M_w}$[b] (g/mol) $\times 10^{-5}$	2.52	2.68
polydispersity ($\overline{M_w/M_n}$)	1.36	1.18

[a] HX-40 was extracted at 40 °C with 1.5 M KOH, and HX-90 was extracted at 90 °C with 1% Ca(OH)$_2$. [b] $\overline{M_w}$ = average molar mass.

($\rho_{DHP} - \rho_{water}$), where ρ_i is the density of compound I, $(dn/dC)_{DHP/DMF}$ is the refractive index increment of the DHP in the DMF, that has been measured to be equal to 0.147,[24] and $\Delta n_{DMF-water}$ is the difference between the refractive indices of the two solvents. Thus the (dn/dC) values used here lie between 0.146 and 0.278 depending on the DHP content of the complexes.

A major difficulty arose when the mixture injected on the SEC was not homogeneous along the elution peak. This was the case for the HX−DHP mixture since we detected that UV elution profiles that represent DHPs (the only UV-absorbing materials) cannot be superimposed to the refractive index elution profiles (total material). DHPs were eluted rather at low elution volumes (high molar mass). Thus the absolute determination of molecular weight would require the calculation of the dn/dC value for each slice studied. This would imply a considerable time-consuming procedure. We ran several simulations using different dn/dC values representing different DHP/HX ratios around the average value calculated for each reaction time. We found that these variations did not drastically change the absolute molecular mass and the molecular mass distribution. Thus, we assumed that the dn/dC values remained constant all over the peak, and we used the values calculated for each DHP/HX ratio. This determination did not interfere with the determination of the root-mean-square (rms) gyration radius ($\langle S^2 \rangle^{1/2}$), the second parameter obtained with MALLS, since this parameter was calculated from the angular dependence of the scattering intensity independently of the concentration determination.[25]

Results

Extraction and Characterization of HX and Synthesis of HX−DHP Complexes. HXs were extracted from maize bran using alkaline extraction at 40 °C with 1.5 M KOH (HX-40) and under more severe conditions at 90 °C with 1% Ca(OH)$_2$ (HX-90).[19] The choice of maize bran instead of other HX sources was guided by two main reasons. The first one is that the maize bran is almost devoid of the lignin[20] that usually contaminates HX samples extracted from lignified samples. The presence of lignin contamination would have introduced artifacts since residual lignin profoundly affects the associative behavior of polysaccharides.[26,27] The second reason is that the maize bran extraction temperature especially modifies the FA content of the samples while other structural parameters such as molar mass, arabinose/xylose ratio, or glucuronic acid content that may influence the studied patterns remain nearly constant (Table 1). Indeed, an increase in temperature leads to the complete deesterification of the FA−arabinose ester linkage whereas at lower temperatures some of the FA moieties are preserved. Thus, with this sample set, we focused our study on a single parameter, which is the FA effect on the supramolecular organization on HX−DHP complexes. FA moieties are sensitive to oxidation and can be coupled to form dehydrodimers, trimers, or tetramers.[6−8] Such polysaccharides cross-coupling results in gel formation when a sufficient HX concentration is used, namely, 0.2−0.4% for wheat or rye flour water-extractable HX[3,28] and 1% for HX-40.[29] In the present study, the HX concentration (0.1%) is rather low compared to those usually used to form gels. However, it is obvious that the first action of the peroxidase used for monolignol polymerization is the oxidation of FA, resulting in the formation of interchain linkages (di-FA or tri-FA). This assumption is supported by the concomitant decrease in the releasable FA monomer content and the increase in dehydrodimer content measured in arabinoxylans after peroxidase treatment (Table 2). Thus, the local formation of a gel or a microgel cannot be ruled out in the case of HX-40 polymerization, and at least local cross-links between HX chains are obvious.

HX−DHP assemblies were obtained through the polymerization of the mono- and dimethoxyaled lignin monomers (coniferyl, G, and sinapyl alcohols, S; Scheme 1) in the HX solution. G and S units are the major monomers of the graminaceous lignin. Thus the reaction mixtures were composed by homo dehydrogenation polymer (DHP-G) from solely gaiacyl monomers or via a 1:1 ratio of coniferyl and sinapyl alcohols (DHP-GS). Polymerization proceeded according the Zutropfverfharen (ZT) method in which the monomers and hydrogen peroxide (enzyme cofactor) are continuously added to a solution of polysaccharides containing the oxidative enzyme. Monolignols are oxidized into radicals that can react either with other monolignols, with the growing DHP polymers, or with feruloylated HX. Indeed, besides the formation of di-FA and tri-FA, ferulate structure can be cross-linked with DHP during the dehydrogenative process.[30] Such a feature is supported by previous works that demonstrated that, during lignification, ferulate structures are incorporated into lignins.[5,30] In our experiments, only 7.0% and 10.5% of the starting FA were identified as monomeric FA or dimers in the HX-40−DHP-G and HX-40−DHP-GS samples. Polymerizations yielded trans-

Table 2. Ferulic Acid, *p*-Coumaric Acid, and Dehydroferulate Release from Heteroxylans (HXs) Following Saponification before and after Monolignol Polymerization[a]

phenol (μg/mg)	HX-40	HX-40−DHP-G	HX-40−DHP-GS	HX-90	HX-90−DHP-G	HX-90−DHP-GS
p-coumaric acid	0.55	0.17	0.089	0.14	0.035	0.017
ferulic acid	3.5	0.704	0.051	0.15	0.072	0.031
5−5′	0.620	0.025	0.044	0	0.0026	0.022
β-0−4	0.180	0.042	0.146	0	0.039	0.049
5−8′	0	0.01	0.17	0	0.08	0.104
total phenol	4.8	0.29	0.5	0.29	0.156	0.223

[a] 5−5′, 8-0−4, and 5−8′ are the three major dehydrodimers of ferulate released from HX extracted from maize bran by alkaline extraction. HX-40 was extracted at 40 °C with 1.5 M KOH, and HX-90 was extracted at 90 °C with 1% Ca(OH)$_2$.

Scheme 1. Heteroxylans Structure and Monolignol Polymerization
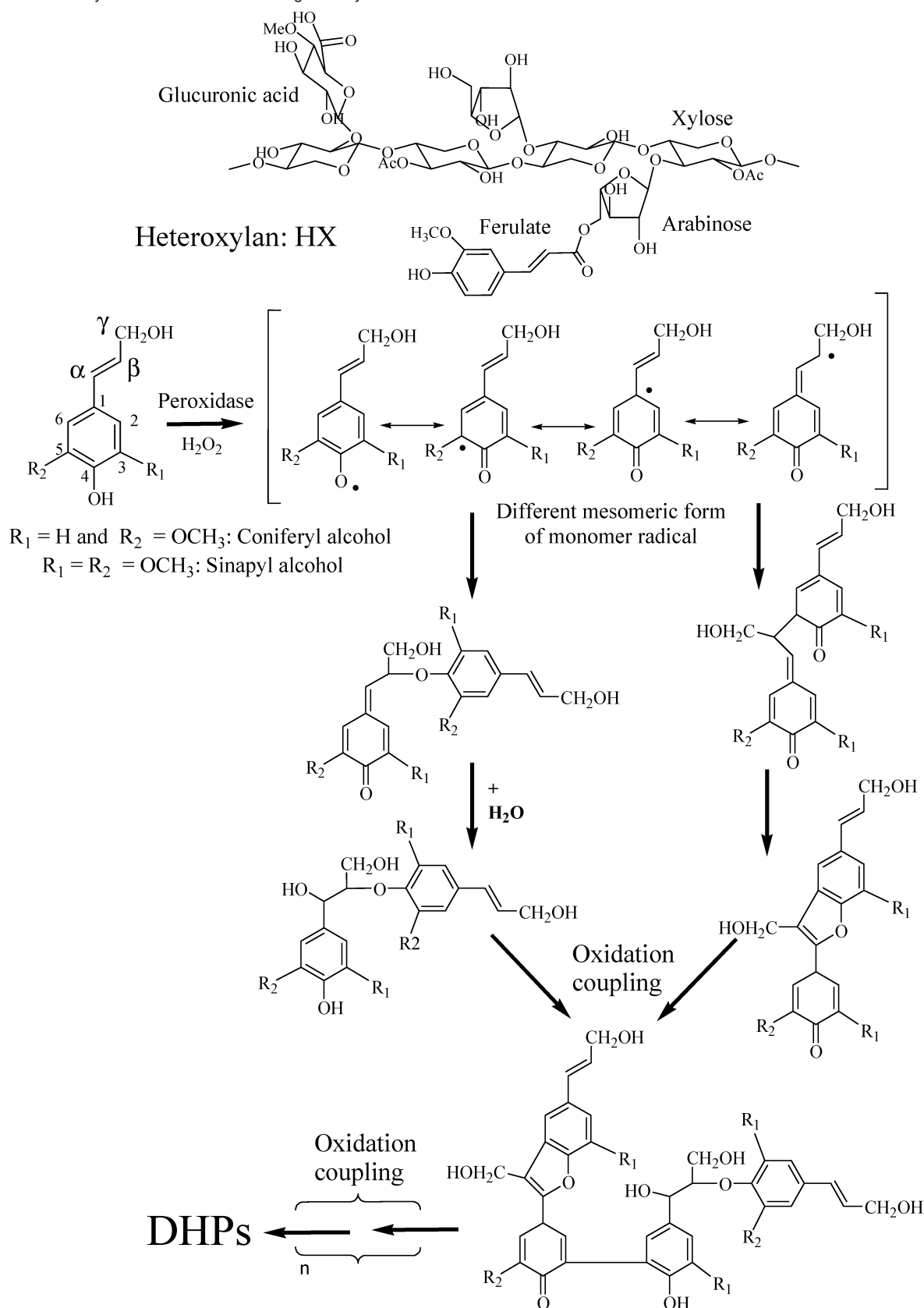
parent colloidal suspensions of HX−DHP in all of the reactions. Suspensions were stable over periods of months.

Morphology and Size Distribution of Particles. A typical image of a negatively stained HX-90−DHP-G preparation is shown in Figure 1a. The particles appear as fairly well individualized spheroidal objects although aggregation is sometimes observed. Images were also recorded from unstained cryo-TEM specimens. As seen in Figure 1b, the shape and size of
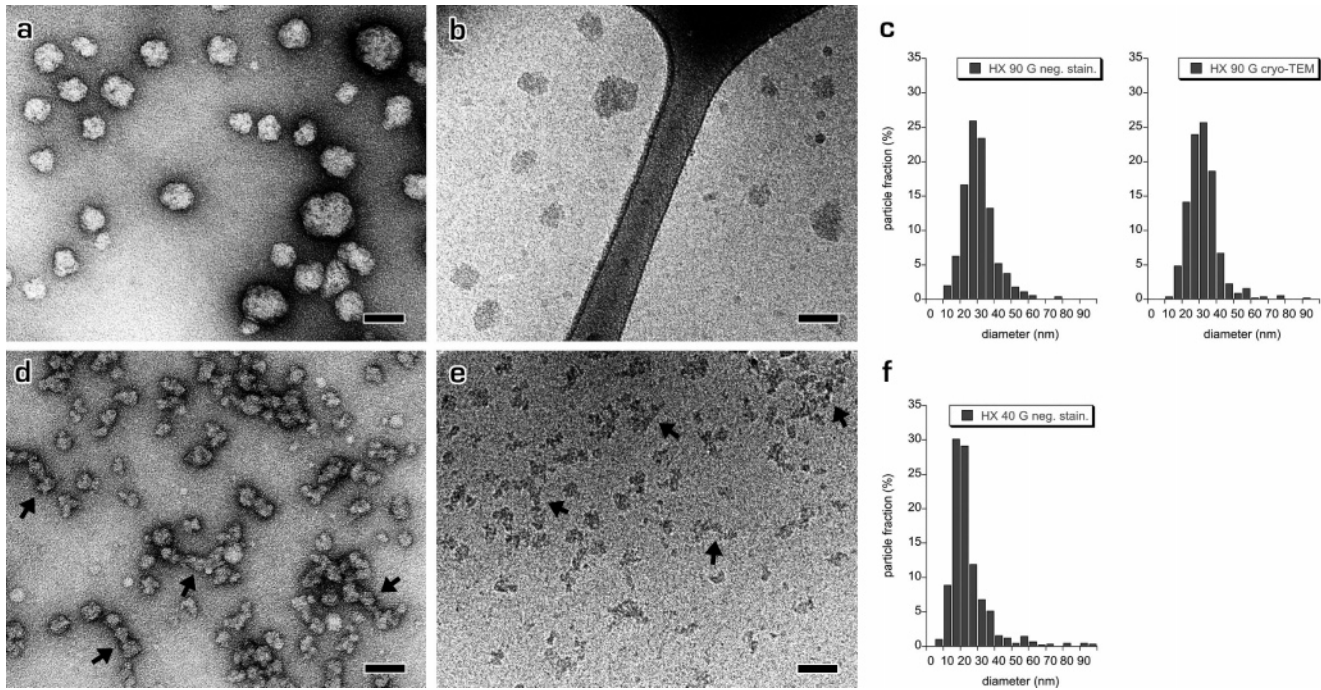
Figure 1. TEM images of (a) negatively stained and (b) ice-embedded HX-90−DHP-G particles (bars, 50 nm); **(c)** corresponding size-distribution histograms. TEM images of (d) negatively stained and (e) ice-embedded HX-40−DHP-G particles (bars, 50 nm). Arrows in part d indicate spheroidal units associated into stringlike objects. Arrows in part e point to similar elongated objects. **(f)** Size-distribution histogram determined from the negatively stained preparation.

HX-90−DHP-G particles embedded in vitreous ice are rather similar to those of dry particles (Figure 1a). No aggregation was detected. Size distribution histograms were determined by measuring the diameters of particles from TEM and cryo-TEM images. The outline of each particle was fitted to an equivalent ellipse. The diameter was calculated as the average between the largest and the lowest diameters of the ellipse. Number and weight average diameters ($\overline{D_n}$ and $\overline{D_w}$, respectively) as well as a polydispersity index P_d were calculated using the expressions presented in ref 31

$$\overline{D_n} = \frac{\sum\limits_i N_i D_i}{\sum\limits_i N_i} \tag{1}$$

$$\overline{D_w} = \frac{\sum\limits_i N_i D_i^4}{\sum\limits_i N_i D_i^3} \tag{2}$$

$$P_d = \frac{\overline{D_w}}{\overline{D_n}} \tag{3}$$

where D_i is the diameter and N_i is the number of particles in the ith class.

The size-distribution histograms corresponding to negatively stained and fast-frozen preparations are shown in Figure 1c. They are asymmetric and extend toward the larger diameters. We calculated $\overline{D_n}$ = 30.8 nm (standard deviation (std) = 9.0 nm), $\overline{D_w}$ = 39.4 nm, and P_d = 1.3 for dry particles and found $\overline{D_n}$ = 25.6 nm (std = 9.1 nm), $\overline{D_w}$ = 40.0 nm, and P_d = 1.5 for

Table 3. Mean Number and Weight Diameters ($\overline{D_n}$ and $\overline{D_w}$, Respectively), Standard Deviation (std, in Brackets), Polydispersity and Connectivity Indices (P_d and C, Respectively) Determined from TEM Images of Negatively Stained and Ice-Embedded Particles (HX-90−DHP-G Only)[a]

sample	$\overline{D_n}$ [std] (nm)	$\overline{D_w}$ (nm)	P_d	C (%)
HX-90−DHP-G (NS)	30.8 [9.0]	39.4	1.3	11.9
HX-90−DHP-G (cryo)	25.6 [9.1]	40.0	1.5	n.d.
HX-90−DHP-GS (NS)	32.0 [15.2]	71.0	2.2	19.3
HX-40−DHP-G (NS)	24.6 [12.2]	55.2	2.2	84.2
HX-40−DHP-GS (NS)	18.4 [16.2]	25.7	1.4	45.5

[a] NS, negative staining; cryo, cryo-TEM; n.d., not determined.

ice-embedded particles (Table 3). The slight difference in $\overline{D_n}$, approximately 5 nm, can be explained by considering that hydrated and soft HX-90−DHP-G particles could flatten to some extent when they dried on the supporting carbon film, resulting in an increase of the apparent particle diameter. However, the difference remains below the standard deviation value (approximately 9 nm).

The objects observed in the HX-40−DHP-G suspension have more complex shapes. Although individual particles can be recognized in images of negatively stained specimens (Figure 1d), they often seem to constitute the basic units of longer stringlike objects. The images of ice-embedded particles show that these elongated objects exist in suspension (Figure 1e) although the shapes of the constituting units cannot be defined with precision. This suggests that this complex feature is not the result of aggregation occurring during the drying process of the negative staining procedure. It is difficult to properly evaluate the sizes of such irregular objects. Using images of negatively stained samples, we measured the diameters of particles as either isolated or elementary units forming the longer strings (see arrows in Figure 1d-). In addition, we defined a

connectivity index C as the percentage of bound objects with respect to the total number of particles measured

$$C = \frac{\sum_i C_i}{\sum_i N_i} \times 100 \qquad (4)$$

where C_i is the connectivity coefficient of particle i and N_i is the number of particles in the ith class. C_i equals 1 if the particle is in contact with one or more neighbor and 0 if it is isolated. The size-distribution histogram of negatively stained HX-40−DHP-G particles is shown in Figure 1f. It is asymmetric toward the larger particles. Number and weight average diameters as well as polydispersity and connectivity indices are summarized in Table 3: $\overline{D}_n = 24.6$ nm (std = 12.2 nm), $\overline{D}_w = 55.2$ nm, $P_d = 2.2$, and $C = 84.2\%$. HX-40−DHP-G elementary particles are thus smaller than those in HX-90−DHP-G and more polydisperse. However, while HX-90−DHP-G particles are mostly individual, those in HX-40−DHP-G seem to be associated into elongated objects.

As seen from images of negatively stained preparations, HX-90−DHP-GS particles also have a spheroidal shape (Figure 2a). The mean diameters and polydispersity index are $\overline{D}_n = 32.0$ nm (std = 15.2 nm), $\overline{D}_w = 71.0$ nm, and $P_d = 2.2$. A significant difference between the size distributions of HX-90−DHP-G and HX-90−DHP-GS was observed. The size distribution of HX-90−DHP-GS is wider than that of HX-90−DHP-G particles, and the polydispersity is higher (Figure 2b). Cryo-TEM images of ice-embedded HX-90−DHP-GS particles were not available for comparison.

The images of negatively stained HX-40−DHP-GS (Figure 2b) particles are rather similar to those from HX-40−DHP-G preparations (Figures 1d and 1e). Some associations of elementary spheroidal objects can be seen, but the number of stringlike aggregates seems lower than that for HX-40−DHP-G, which is confirmed by the lower connectivity index $C = 45.5\%$. We measured $\overline{D}_n = 18.4$ nm (std = 16.2 nm), $\overline{D}_w = 25.7$ nm, and $P_d = 1.4$. Basic elements are thus smaller and less polydisperse than in the case of HX-40−DHP-G.

Size Exclusion Chromatography with Online Multiangle Laser Light Scattering. Besides the morphological characterization obtained from TEM images, we used size exclusion chromatography with online multiangle laser light scattering to obtain information on the organization of the particles and their evolution during polymerization. Samples were analyzed at different reaction times (0, 10, 30, 60, and 240 min). The particles analyzed by TEM correspond to the sample taken at 240 min. For all injections, we estimated the amount of products analyzed by calculating the recovery percentage (Table 3). This parameter estimates an estimation of the loss of products due to sample filtration before elution and also adsorption phenomena that may occur during elution. In almost all cases, the percentage recovery represents a significant part of the amount injected, thus demonstrating the significance of the results. Light scattering enables the determination of the average number and weight molar masses ($\overline{M}_n$ and $\overline{M}_w$, respectively) and the root-mean-square gyration radius ($\langle S^2 \rangle^{1/2}$). These parameters are independent of any calibration or reference standards. The first one requires the polymer concentration during the elution whereas the second one is calculated from the angular dependence of the scattering intensity.[25] In the case of polydisperse samples, the relationship between the polymer dimensions and
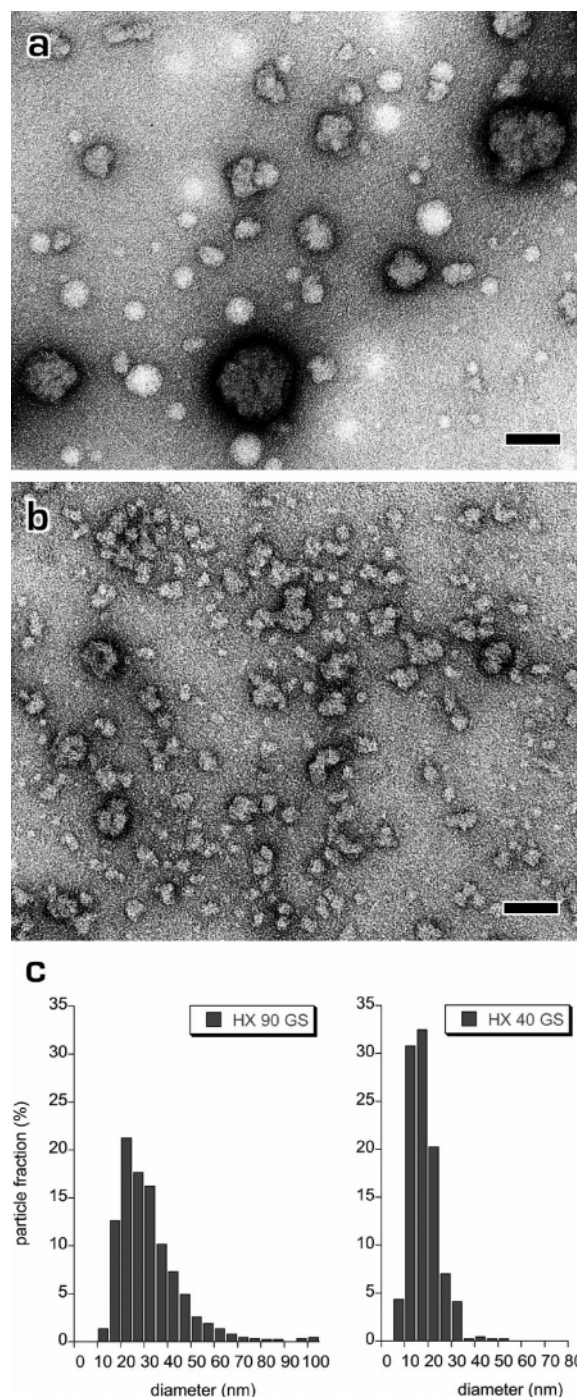

Figure 2. TEM images of (a) HX-90−DHP-GS and (b) HX-40−DHP-GS particles negatively stained with uranyl acetate (bars, 50 nm); **(c)** corresponding size-distribution histograms.

the molecular weight (M) can be obtained. This relation is usually described as a scaling law of the form

$$\langle S^2 \rangle^{1/2} = QM^q \qquad (5)$$

The power law exponent q is related to the shape of the chain and gives information about the polymer−solvent interactions and macromolecular conformations of the polymer. Values ranging from 0.5 to 0.6 are predicted for random-coil polymers in rather good solvent conditions. Rigid rod polymers present q values as high as 1 whereas spherical particles have a q value equal to 0.3. Values below 0.3 indicate a complex conformation
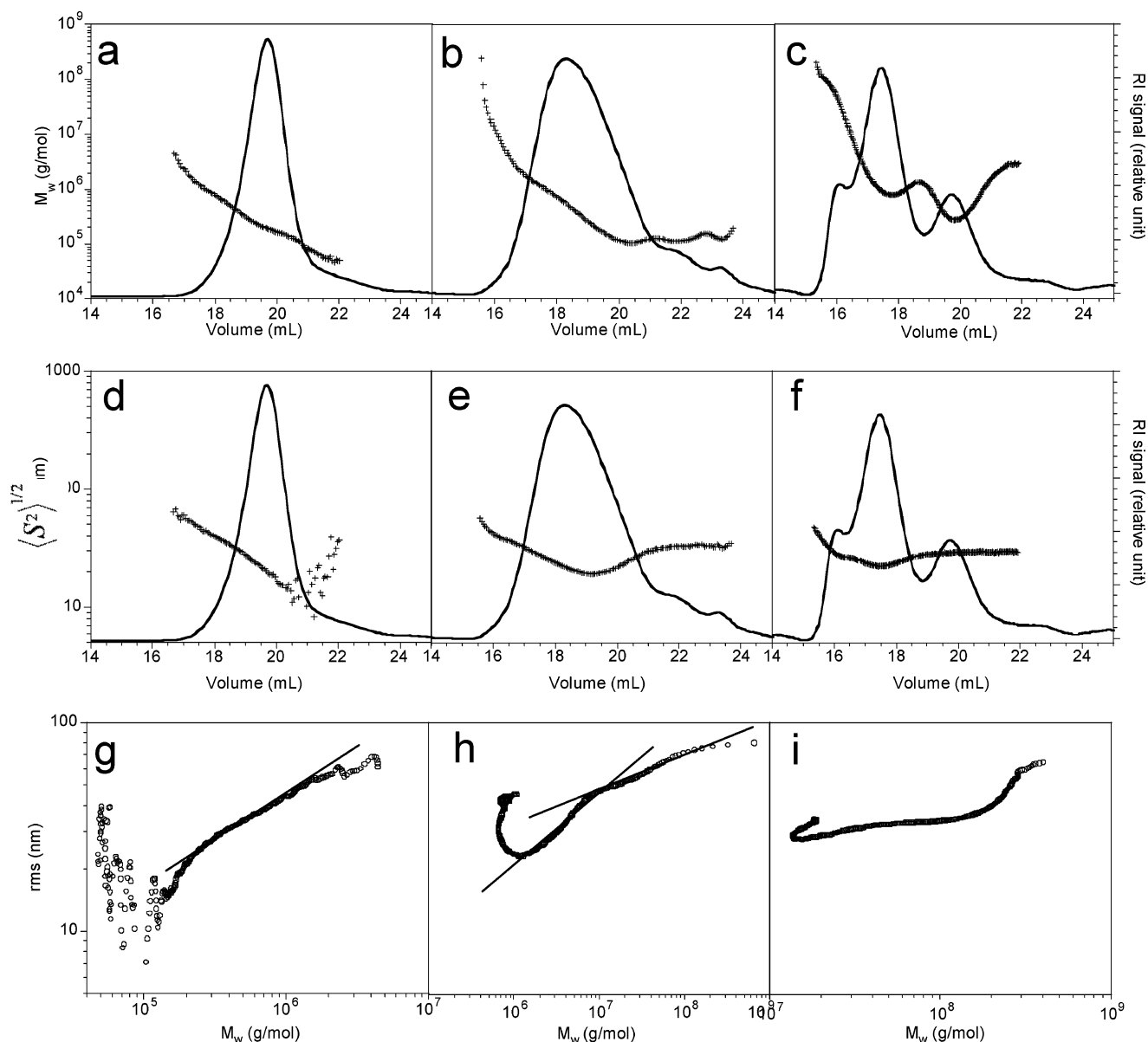
Figure 3. (a, b, c) and (d, e, f) distributions and scaling law (g, h, i) (log-log plot versus) for HX-40-DHP-G at reaction time $t = 0$ (a, d, g), 30 (b, e, h), and 240 min (c, f, i). Average molecular mass in weight (g/mol) root mean square radius of gyration (nm).

and highly polydisperse samples that may reflect more complex patterns such as aggregated particles.[25]

Before the reaction starts, HX-40 presents a unique eluted peak that displays a regular evolution of both $\overline{M_w}$ and $\langle S^2 \rangle^{1/2}$ over the elution curve. The log−log plot of $\overline{M_w}$ versus $\langle S^2 \rangle^{1/2}$ is nearly fully linear except for the lowest molar mass values since the $\langle S^2 \rangle^{1/2}$ value measured is very close to the lowest limit of detection of the system (10 nm), resulting in a noisy signal. The fit of the linear part of the scaling law plot has a slope value (q) roughly equal to 0.5 indicating that HX is in rather good solvent conditions in the chromatographic solvent in good agreement with previous measurements.[23]

Figures 3d−3f display $\overline{M_w}$ and $\langle S^2 \rangle^{1/2}$ distributions at a reaction time of 30 min. Both parameters show an unusual distribution. In the first part of the elution curve (before 19 min), $\overline{M_w}$ and $\langle S^2 \rangle^{1/2}$ decrease with the elution in agreement with the SEC process, while after 19 min those parameters increase contrary to classical SEC profiles (Figures 3d and 3e). This effect induces a curvature of the scaling law plots at the low molar values (Figure 3f). Such an anomalous elution behavior

has already been observed for polyphosphagene,[32,33] dendrimers,[34] and biopolymer microgels.[25] In these previous works, this phenomenon was attributed to the occurrence of an extremely high molar mass fraction, such as a microgel or highly branched molecules, trapped in the column material and eluted at volumes higher than expected by the pure SEC process. This high molar mass fraction coelutes with smaller size molecules that follow the separation mechanism based on normal size exclusion increasing the polydispersity of each slice. According to the proportion of high and low mass fractions, $\overline{M_w}$ and $\langle S^2 \rangle^{1/2}$ increase or remain stable resulting in the upturn observed in the scaling law plots. Such behavior has been demonstrated in all HX−DHP samples suggesting the formation of gel structures. Such a hypothesis is consistent with the chemical structure of HX-40 since feruloylated HX is able to form a gel in the presence of an oxidative enzyme.[28] However, gel formation cannot be so easily deduced in the case of HX-90 samples since they are devoid of FA; it has to be assumed that the formation of large branched structures may occur during the polymerization of monolignols.
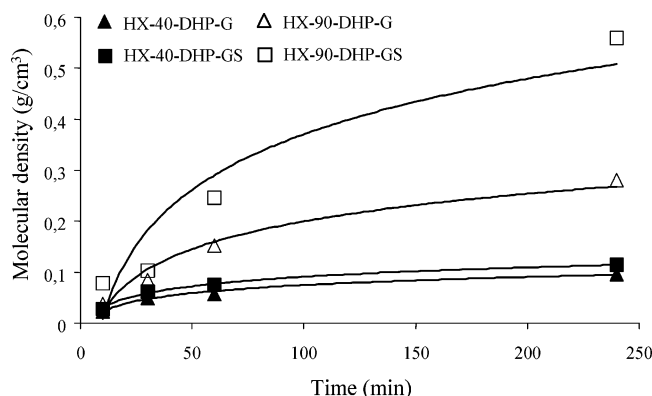
Figure 4. Variation with reaction time of the molecular density (($\rho = \overline{M_w}/N_{A^*}(\langle S^2\rangle^{1/2})^3$) for HX-40−DHP-G (triangles), HX-40−DHP-GS (squares), HX-90−DHP-G (open triangles), and HX-90−DHP-GS (open squares): $\overline{M_w}$, average molecular mass in weight; $\langle S^2\rangle^{1/2}$, root-mean-square radius of gyration (nm). Lines are guides for the eyes.

Besides this anomalous behavior, at lower elution volumes, molar mass and $\langle S^2\rangle^{1/2}$ behave as expected in classical SEC elution profiles (Figures 4d and 4e). Thus scaling law exponents can be calculated since two linear zones can be identified and fitted. In the first one (intermediate molar mass range), a q value of 0.48 is obtained, indicating that a part of the polymer is still in good solvent conditions (Table 3). In the highest molar mass zone, the q value is nearly equal to 0.3 (Table 4), indicating the formation of dense spheres. Since this part presents the highest concentrations of DHPs as demonstrated by the UV elution profiles (data not shown), the formation of denser structures can be related to the polymerization of monolignols. Indeed such a collapse was already demonstrated during coniferyl alcohol polymerization in the presence of pectin using light and neutron scattering.[35]

At the longest reaction time, the elution pattern becomes more complex (Figures 3g−3i). Increases of $\overline{M_w}$ and $\langle S^2\rangle^{1/2}$ at low elution volumes are still visible, inducing the upturn of the scaling law process. At higher molar masses, all of the zones of the scaling law plots display q values lower than 0.3. The feature can be interpreted as the collapse of the HX−DHP structures in dense particles with complex shapes and organization.

Table 4 summarizes all of the values measured for four samples at different reaction times. Both $\overline{M_w}$ and $\langle S^2\rangle^{1/2}$ increase during the reaction. All along the reaction, the highest values were measured for the HX-40 samples at the opposites of the results obtained by TEM. SEC-MALLS data yield also other information on the formation of HX−DHP nanoparticles. Indeed the decrease of the q exponent of the scaling law from a value of 0.5 to 0.3 then finally less than 0.3 indicates that particles collapse during the polymerization and undergo a significant densification. This is also demonstrated by the increase of the molecular density $\rho = M_w/(\langle S^2\rangle^{1/2})^3$ all along the reaction that is an indication of the densification of the particles (amounts of matter by unit of volume) (Figure 4). A similar trend was already demonstrated by model approaches in the case of pectin−DHP complexes.[35] Values reported here are in good agreement with those calculated for pectin−DHP complexes ($\rho = 0.21$ g/cm³) with a 1:1 pectin/DHP complex[35] but also for natural polymers such as glycogen ($\rho = 0.19$ g/cm³).[36] Such a collapse was suggested by in vivo study.[37] However, evolutions of the HX−DHP densities are not identical for all of the complexes, and again HX-40 and HX-90 samples behave differently. The non-feruloylated samples reach density values higher than that of HX-40 (Figure 4).

Discussion

The particle sizes obtained by TEM and MALLS at the end of the reaction (240 min) are significantly different. Indeed, SEC-MALLS values are 3−5 times larger than the TEM ones, whereas it has been shown in the case of phytoglycogen particles that a good agreement could be found between the results of these two techniques.[31] Moreover rank order is also changed. Indeed the HX-40 samples have larger $\langle S^2\rangle^{1/2}$ values than the HX-90 ones, contrary to the results found in the TEM measurements. These differences can be explained by a combination of two reasons:

The first one is related to the calculation method chosen in the TEM approach. Since complex HX-40 sample shapes could not be properly evaluated, we measured the size of circular subunits. This measurement neglected the real sizes of the elongated objects or larger aggregates. Cryo-TEM images showed that stringlike objects existed in suspension and did not systematically result from a drying artifact. Moreover HX-90

Table 4. SEC MALLS Data Calculated for HX−DHP Samples during the Polymerization Reaction

time (min)		HX-40−DHP-G	HX-40−DHP-GS	HX-90−DHP-G	HX-90−DHP-GS
0	$\overline{M_w}$ (g/mol); P; R (%)	2.52×10^5; 1.36; 86		2.68×10^5; 1.18; 95	
	rms (nm)		19		24
	q^b		0.5		0.48
10	$\overline{M_w}$ (g/mol); P; R (%)	6.36×10^5; 3.5; 82	8.5×10^5; 2.7; 73	1.12×10^6; 2.96; 70	1.58×10^6; 3.1; 94
	rms (nm)	37.8	37	37	<10
	q^b	0.42	0.32	0.3/<0.3	
30	$\overline{M_w}$ (g/mol); P; R (%)	2.01×10^6; 2.15; 62	3.04×10^6; 1.92; 53	1.13×10^6; 3.2; 77	7.7×10^6; 2.9; 50
	rms (nm)	40.8	43	27	27
	q^b	0.48/<0.3	0.35/<0.3	0.35/0.3	<0.3
60	$\overline{M_w}$ (g/mol); P; R (%)	2.96×10^6; 1.75; 60	7.45×10^6; 1.83; 49	2.07×10^6; 2.16; 60	1.11×10^7; 2; 49
	rms (nm)	43.5	47.5	28	42
	q^b	0.42/<0.3	0.37/<0.3	<0.3	<0.3
240	$\overline{M_w}$ (g/mol); P; R (%)	1.43×10^7; 1.38; 55	9.09×10^6; 1.92; 53	1.33×10^7; 1.4; 61	3.3×10^7; 1.8; 48
	rms (nm)	63	52	39	47
	q^b	<0.3	<0.3	<0.3	<0.3

[a] $\overline{M_w}$, average molar mass; P, polydispersity ($\overline{M_w}/\overline{M_n}$); R, percentage of recovery (amounts of eluted product calculated from the dn/dC divided by the amount of injected product); rms, root-mean-square radius of gyration; q, power law exponent. [b] When several conformations exist, q is calculated for each conformation starting from low to high molecular mass.

Scheme 2. Formation of HX-90−DHP and HX-40−DHP Nanoparticles[a]

HX 40   HX 90

a

b

c

⟨°°°°°°°°°°°⟩ HX   ° Ferulic acid   ○ DHPs
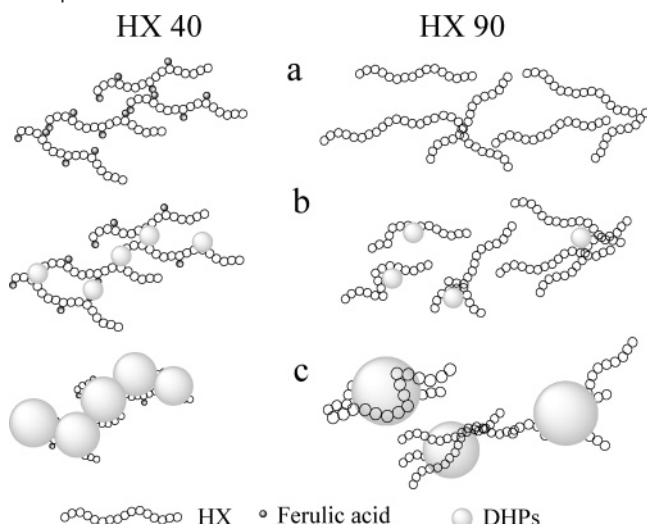
[a] In step a, the ferulic acid substituents of HX-40 are cross-linked via ferulic bridges while HX-90 behaves as free chains. In step b, DHP nodules are formed and can be connected to the ferulate structure of HX-40. DHPs induce the aggregation of HX-40 and HX-90. In step c, the polymerization is complete. HX-40−DHPs form stringlike objects while HX-90−DHPs behave as more individual particles. Objects are also larger and denser since particles can coalesce and polymers can be more easily reorganized.

samples that have a very close chemical structure did not form such an association. Thus, the subunits measured in TEM are certainly not dissociated in SEC, leading to larger sizes and explaining the inversion of the size rank order. In depth analysis of size and shape of such heterogeneous and complex objects has to be considered in future work, in particular by observing TEM preparations from highly dilute samples, thus preventing any aggregation artifacts. This point supports the conclusion that elongated objects may result from covalent linkages between the elementary objects observed by TEM. Thus, this feature must be related to the feruloylation level that is the main structural difference between the two samples.

The second reason that may explain the divergence of the TEM and SEC-MALLS results is related to the occurrence of microgels or highly branched structure. Indeed, such products may also contribute to the significant increase in size measured by SEC. These structures that are demonstrated by the anomalous elution profile previously discussed may have a very low density and thus may be hardly detectable by TEM. However, they can induce higher $\langle S^2 \rangle^{1/2}$ values. This local gel formation is likely favored in the case of HX-40 samples since they contain the highest FA content.

These results clearly demonstrated the effect of the chemical structure of the preexisting polysaccharide network on the buildup of supramolecular architecture of lignin-like/polysaccharide complexes. Indeed, FA substitution that is equal to 0.29 for HX-90 and 4.85 μg/mg for HX-40, corresponding roughly to 0.3 and 5 FA residues per 1000 xylose residues, respectively, induces important differences in the morphology and supramolecular characteristics of HX−DHP nanoparticles. As observed by TEM, the morphology of particles obtained from the highly FA-substituted HX display more complex organizations. The main pattern observed is the formation of stringlike objects composed of spheroidal elementary units whereas less feruloylated HX behaves more as individual particles. The latter particles were found to be denser than the first one. Such differences must be related to the FA reactivity. Previous works

have demonstrated that during lignification, the cell wall becomes cross-linked by dehydrogenation of ferulate monomers and by incorporation of ferulate monomers and dehydrodimers into lignins.[5] This result implies that FAs either cross-link the HX chains and/or act as nucleation points for lignin monomers in agreement with previous results.[38] Assuming that a similar behavior took place in our model experiments would mean that DHPs are anchored to HX in the HX-40 sample. The exact mechanism has to be determined since it could be attributed either to cross-coupling between DHPs and ferulates or to the formation of a preexisting network with FA dimer formation creating hydrophobic domains where DHPs polymerization may be favored. Whatever the mechanism, the growth of DHP molecules/aggregates is favored and promoted by FA, resulting in cross-linking of DHP particles on HX chains. As a consequence, DHP particles can be interlinked by HX chains, since two different FA moieties of a single HX chain may react with two different DHP particles. Thus, when growth and densification of DHP particles occur, they connect to each other and form the stringlike structures. Such intra- and interparticle connections may induce steric hindrance due to entanglement of chains limiting their ability to reorganize. Such processes may limit the densification phenomena. The lack of FA may allow particle densification.

Beside the of FA effect, syringyl monomers also seem to have a certain impact on particle densification since GS particles reach a higher condensation level in both feruloylated and non-feruloylated samples (Figure 4). This result is supported by the decrease of the q exponent observed at early reaction times in the case of the polymerization of a GS mixture (Table 3). This finding may indicate that syringyl monomers present a higher affinity for the HX than the G ones. This point will require a future in depth investigation.

The results show the role of the phenolic substitution on the construction of the supramolecular organization of HX−lignin-like composites. In vivo, such a parameter may be crucial to control of the ultrastructural organization of lignin. Indeed, the HX−FA network may act as a scaffold and a template for the lignin polymer growth. Thus besides the chemical importance of FA, the control of the distribution and the amount of the FA substitution can be proposed as a means for genetic machinery to control the buildup of cell wall elements and the resulting properties of this composites. These results also emphasize the highly efficient interactions occurring between xylans and lignins, as already suggested for wood samples.[39] These findings support the hypothesis that xylans are intimately linked with the lignin network.

References and Notes

(1) Boudet, A. M. In *The Plant Cell Wall*; Rose, J. K. C., Eds., Blackwell Publishing: Oxford, U. K., 2003; pp 155−178.

(2) Fratzl, P.; Burgert, I.; Gupta, H. S. *Phys. Chem. Chem. Phys.* **2004**, *6*, 5575.

(3) Izydorczyk, M. S.; Biliaderis, C. G. *Carbohydr. Polym.* **1995**, *28*, 33.

(4) Ishii, T. *Plant Sci.* **1997**, *127*, 111.

(5) Grabber, J. H.; Ralph, J.; Hatfield, R. D. *J. Agric. Food Chem.* **2000**, *48*, 6106.

(6) Carvajal-Millan, E.; Guigliarelli, B.; Belle, V.; Rouau, X.; Micard, V. *Carbohydr. Polym.* **2005**, *59*, 181.

(7) Bunzel, M.; Ralph, J.; Bruning, P.; Steinhart, H. *J. Agric. Food Chem.* **2006**, *54*, 6409.

(8) Bunzel, M.; Ralph, J.; Funk, C.; Steinhart, H. *Tetrahedron Lett.* **2005**, *46*, 5845.

(9) Rouau, X.; Cheynier, V.; Surget, A.; Gloux, D.; Barron, C.; Meudec, E.; Louis-Montero, J.; Criton, M. *Phytochemistry* **2003**, *63*, 899.

(10) Ralph, J.; Quideau, S.; Grabber, J. H.; Hatfield, R. H. *J. Chem. Soc., Perkin Trans. 1* **1994**, 3845.

(11) Saulnier, L.; Crepeau, M. J.; Lahaye, M.; Thibault, J. F.; Garcia-Conesa, M. T.; Kroon, P. A.; Williamson, G. *Carbohydr. Res.* **1999**, *320*, 82.

(12) Jacquet, G.; Pollet, B.; Lapierre, C.; Mhamdi, F.; Rolando, C. *J. Agric. Food Chem.* **1995**, 43, 2746.

(13) Tanahashi, M.; Higuchi, T. *Wood Res.* **1981**, *67*, 29.

(14) Higuchi, T.; Ogino, K.; Tanahashi, M. *Wood Res.* **1971**, *51*, 1.

(15) Grabber, J. H.; Hatfielfd, R. D.; Ralph, J.; Zon, J.; Amrhein, N. *Phytochemistry* **1995**, *40*, 1077.

(16) Grabber, J. H.; Ralph, J.; Hatfield, R. D.; Quideau, S.; Kuster, T.; Pell, A. N. *J. Agric. Food Chem.* **1996**, *44*, 1453.

(17) Kerr, E. M.; Fry, S. C. *Planta* **2004**, *219*, 73.

(18) Fry, S. C. *New Phytol.* **2004**, *161*, 641.

(19) Chanliaud, E.; Saulnier, L.; Thibault, J. F. *J. Cereal Sci.* **1995**, *21*, 195.

(20) Lapierre, C.; Pollet, B.; Ralet, M.-C.; Saulnier, L. *Phytochemistry* **2001**, *57*, 765.

(21) Ludley, F. H.; Ralph, J. *J. Agric. Food Chem.* **1996**, *44*, 2942.

(22) Harris, J. R. In *The Thin Film Techniques*; Bios Scientific Publishers: Oxford, U. K., 1977.

(23) Chanliaud, E.; Roger, P.; Saulnier, L.; Thibault, J. F. *Carbohydr. Polym.* **1996**, *31*, 41.

(24) Cathala, B.; Saake, B.; Faix, O.; Monties, B. *J. Chromatogr., A* **2003**, *1020*, 229.

(25) Wyatt, P. J. *Anal. Chim. Acta.* **1993**, *272*, 1.

(26) Saake, B.; Kruse, T.; Puls, J. *Bioresour. Technol.* **2001**, *80*, 195.

(27) Linder, A.; Bergman, R.; Bodin, A.; Gatenholm, P. *Langmuir* **2003**, 19, 5072.

(28) Carvajal-Millan, E.; Guilbert, S.; Doublier, J. L.; Micard, V. *Food Hydrocolloids* **2006**, *20*, 53.

(29) Dervilly-Pinel, G.; Rimsten, L.; Saulnier, L.; Andersson, R.; Aman, P. *J. Cereal Sci.* **2001**, *34*, 207.

(30) Ralph, J.; Helm, R. F.; Quideau, S. *J. Chem. Soc., Perkin Trans. 1* **1992**, *21*, 2971.

(31) Putaux, J. L.; Buleon, A.; Borsali, R.; Chanzy, H. *Int. J. Biol. Macromol.* **1999**, *26*, 145.

(32) Laguna, M. T. R.; Saiz, E.; Tarazona, M. P. *Polymer* **2000**, *41*, 7993.

(33) Laguna, M. T. R.; Tarazona, M. P. *Polymer* **2001**, *42*, 1751.

(34) Percec, V.; Ahn, C. H.; Cho, W. D.; Jamieson, A. M.; Kim, J.; Leman, T.; Schmidt, M.; Gerle, M.; Moller, M.; Prokhorova, S. A.; Sheiko, S. S.; Cheng, S. Z. D.; Zhang, A.; Ungar, G.; Yeardley, D. J. P. *J. Am. Chem. Soc.* **1998**, *120*, 8619.

(35) Lairez, D.; Cathala, B.; Monties, B.; Bedos-Belval, F.; Duran, D.; Gorrichon, L. *Biomacromolecules* **2005**, *6*, 763.

(36) Yoo, S. H.; Jane, J. L. *Carbohydr. Polym.* **2002**, *49*, 307.

(37) Terashima, N.; Awano, T.; Takabe, K.; Yoshida, M. *C. R. Biol.* **2004**, *327*, 903.

(38) Ralph, J.; Grabber, J. H.; Hatfield, R. D. *Carbohydr. Res.* **1995**, *275*, 167.

(39) Salmen, L.; Olsson, A. M. *J. Pulp Pap. Sci.* **1998**, *24*, 99.